MNRAS **000**, 1–11 (2015) Preprint 1 December 2015 Compiled using MNRAS LATEX style file v3.0

A large, long-lived structure near the trojan L5 point in the post common-envelope binary SDSS J1021+1744

P. Irawati[1,⋆] A. Richichi[1], M. C. P. Bours[2], T. R. Marsh[3], N. Sanguansak[4], K. Chanthorn[4], J. J. Hermes[2], L. K. Hardy[5], S. G. Parsons[2], V. S. Dhillon[5,6], S. P. Littlefair[5]

[1]*National Astronomical Research Institute of Thailand, 191 Siriphanich Bldg., Huay Kaew Road, Chiang Mai 50200, Thailand*
[2]*Departamento de Física y Astronomía, Universidad de Valparaíso, Avenida Gran Bretaña 1111, Valparaíso, Chile*
[3]*Department of Physics, University of Warwick, Gibbet Hill Road, Coventry CV4 7AL, UK*
[4]*School of Physics, Suranaree University of Technology, 111 University Avenue, Muang, Nakhon Ratchasima 30000, Thailand*
[5]*Department of Physics and Astronomy, University of Sheffield, Sheffield S3 7RH, UK*
[6]*Instituto de Astrofísica de Canarias, 38205 La Laguna, Santa Cruz de Tenerife, Spain*

arXiv:1511.09205v1 [astro-ph.SR] 30 Nov 2015

Accepted 2015 November 27. Received 2015 November 27; in original form 2015 September 18

ABSTRACT

SDSS J1021+1744 is a detached, eclipsing white dwarf / M dwarf binary discovered in the Sloan Digital Sky Survey. Outside the primary eclipse, the light curves of such systems are usually smooth and characterised by low-level variations caused by tidal distortion and heating of the M star component. Early data on SDSS J1021+1744 obtained in June 2012 was unusual in showing a dip in flux of uncertain origin shortly after the white dwarf's eclipse. Here we present high-time resolution, multi-wavelength observations of 35 more eclipses over 1.3 years, showing that the dip has a lifetime extending over many orbits. Moreover the "dip" is in fact a series of dips that vary in depth, number and position, although they are always placed in the phase interval 1.06 to 1.26 after the white dwarf's eclipse, near the L5 point in this system. Since SDSS J1021+1744 is a detached binary, it follows that the dips are caused by the transit of the white dwarf by material around the Lagrangian L5 point. A possible interpretation is that they are the signatures of prominences, a phenomenon already known from Hα observations of rapidly rotating single stars as well as binaries. What makes SDSS J1021+1744 peculiar is that the material is dense enough to block continuum light. The dips appear to have finally faded out around 2015 May after the first detection by Parsons et al. in 2012, suggesting a lifetime of years.

Key words: binaries: close – binaries: eclipsing – stars: white dwarfs – stars: individual: SDSS J102102.25+174439.9

1 INTRODUCTION

In recent years, primarily as the result of the Sloan Digital Sky Survey (SDSS, York et al. 2000; Abazajian et al. 2009), large numbers of white dwarf / main-sequence (WDMS) binaries have been discovered (Rebassa-Mansergas et al. 2007, 2012, 2013). A significant number of these have periods so short that they must have emerged from a phase in which both stars orbited within the envelope of the white dwarf's progenitor. During such "common envelope" phases, binary orbital energy is lost to the envelope (Webbink 1984), resulting in the observed short-periods (or often complete merging of the stars, Briggs et al. 2015). White dwarf / main-sequence post common-envelope binaries (PCEBs) form a large, easily observed population for testing the outcome of the common-envelope phase, which is significant in the formation of many classes of close binary.

As the number of known PCEBs has increased, so too has the number of eclipsing systems. Thus, while in 2000 we knew of just 5 eclipsing PCEBs (Marsh 2000, including the WD + K dwarf system V471 Tau), the most recent census (Parsons et al. 2015) lists 71 such systems. Amongst these is the subject of the present paper, SDSS J102102.25+174439.9 (hereafter J1021+1744). J1021+1744 was first recognized as

⋆ E-mail: puji.irawati@narit.or.th

© 2015 The Authors

a WDMS binary from the SDSS Data Release 7 and the stellar parameters of this binary were published as part of the online SDSS WDMS binary catalogue (http://www.sdss-wdms.org, Rebassa-Mansergas et al. 2012). This binary was also suspected as strong candidate PCEB from its radial velocity variability. The catalogue published an M4 type for the red dwarf star and a white dwarf with mass of $1.06 \pm 0.087\,M_{\odot}$. The effective temperature of the white dwarf in J1021+1744 was given as 'hot' and 'cold' solution from the Balmer line profile fits. The white dwarf temperatures are 32595 ± 928 K and 17505 ± 820 K for the hot and cold case, respectively.

The eclipsing nature of J1021+1744 was discovered by Parsons et al. (2013, P13 hereafter) from a search for photometric variability of WDMS systems in Catalina Sky Survey (CSS, Drake et al. 2009, 2014) data. The eclipses are of the white dwarf by its M dwarf companion and recur with an orbital period of 0.14 days. Using the robotic Liverpool Telescope (LT) in 2012 June, P13 found a drop in the brightness shortly after eclipse, about half as deep as the eclipse itself. This is highly unusual: outside eclipse, the vast majority of these systems show only slow variations due to irradiation and tidal distortion. P13 showed a possible flare taking place before the white dwarf was fully out of the eclipse, leading them to suggest that the dip in flux might be caused by material ejected from the flare. They gave new constraints for the white dwarf mass using their new ephemeris data, the measured radial velocity, and the mass function equation, lowering the estimated mass to $0.50 \pm 0.05\,M_{\odot}$. Rebassa-Mansergas et al. (2012)'s white dwarf mass was based upon model atmosphere fitting, made difficult because of the contamination of the white dwarf's spectrum by its companion.

In this paper we present photometric observations of J1021+1744 taken mainly with the 2.4 m telescope at the Thai National Observatory, covering more than 30 eclipses from 2014 January to 2015 May in a variety of filters and with sub-minute time resolution. Our observations reveal that the dip observed by P13 is long-lived, with a lifetime of at least a few years. We also show that the dip is resolved into multiple components that vary both with time and wavelength. We suggest here that the dips originate from obscuration of the white dwarf showing that this detached binary is able to support dense clouds of material around the L5 trojan point.

2 OBSERVATIONS AND DATA REDUCTION

The bulk of our photometric data of J1021+1744 were taken using the 2.4 m Thai National Telescope (TNT) on Doi Inthanon, equipped with the ULTRASPEC camera. This facility is ideal for such studies, thanks to the combination of high time resolution, sensitivity and flexibility in time allocation. We supplemented this with a single eclipse observed with the high-speed triple-beam camera ULTRACAM mounted on the 4.2m William Herschel Telescope (WHT) on 2015 January 17. ULTRASPEC is based on a low-noise 1k × 1k EMCCD frame-transfer detector, and is described in detail by Dhillon et al. (2014). During the first observing cycle of TNT (2013 November – 2014 April), we monitored this star for 17 nights from 2014 January to April, covering more than 20 eclipses in different filters. In the following cycle (2014 November – 2015 May), we obtained 13 more eclipses from 9 nights of observations. The log of our observations is presented in Table 1.

Each observation consists of several hundreds to several thousands of frames, with the sampling times listed in Table 1. The detector integration times are 14.9 ms shorter than the sampling times (see section 3.4 of Dhillon et al. 2014). The frame size is usually equal to the full detector window, although in some cases smaller windows are adopted (e.g. 400×800 pixels). Each frame is accurately time-stamped at mid-exposure thanks to a dedicated GPS system. The data are then processed using the ULTRACAM pipeline (Dhillon et al. 2007). After bias subtraction and flat fielding, the data are corrected to take into account the position of the Solar System Barycenter. One or more reference stars are recorded simultaneously with J1021+1744, allowing us to obtain accurate relative photometry. We note that the ULTRACAM pipeline includes adaptive estimates of seeing and star positions, and is thus very robust against changes in photometric quality, airmass, and tracking errors.

For our observations we used several ULTRASPEC filters which are similar to the passbands of the SDSS photometric system, namely g', r', i', z'. Additionally, we used the KG5 filter which is effectively equivalent to SDSS $u'+g'+r'$ (as described in Dhillon et al. 2014), and the self-explanatory $i'+z'$ filter. Finally, we also obtained data with a clear filter (white light).

During the data processing we noticed several inconsistencies in the depth of the primary eclipses. Eclipses in white dwarf binaries are wavelength dependent, and we realized that some of our light curves supposedly taken with the same filter appear to have different eclipse depths. Further investigations indicated that there were problems with the filter wheel rotation on some of our nights. In other words, the wheel did not move to the intended filter, without any alerts at the software level. We recovered from the problem as follows.

For each of the data sets with an ambiguous filters, we stacked all frames to create one deep image and examined all non-variable stars in the field. We then compared the fluxes against various sky surveys. Using this method we could identify the correct filter for all of our affected data. We also verified the eclipse depths by filter, as discussed in Section 3. The changes from nominal to adopted filters are marked in Table 1. The problem was fixed at the hardware level in the summer of 2014 and is not present in later data.

In Table 1 we list the signal-to-noise ratio (SNR) as computed over 10 minutes in the pre-eclipse part of the light curve, centered around phase 0.93. The numbers in the seeing column are approximate values measured from the stellar profiles.

3 PHOTOMETRIC ANALYSIS

3.1 Light curve fitting

We implemented a light curve fitting method (Copperwheat et al. 2010) to obtain the parameters for our binary model. To find the best parameters of the model, we first fit all light curves with the same filter using

Table 1. Observation log of J1021+1744 obtained from TNT using ULTRASPEC and WHT with ULTRACAM. Each row represents one dataset where the start and the end of the exposure are given in columns 4 and 5, together with the corresponding orbital phase in column 6. The filters are listed in column 7. The presence of a colon before the filter denotes that the nominal filter name has been changed to an adopted filter, as explained in the text. Column 8 gives the exposure time of a single frame, where there is a dead time of 14.9 ms between exposures. In Column 9 and 10 we list SNR (measured in the pre-eclipse part; see text) and approximate seeing values for each run.

No	Date	Telescope	UT start	UT end	Orbital Phase coverage	Filter	Sampling (sec)	SNR	Seeing ($''$)
1	2014 Jan 07	TNT	20:27:49	22:10:17	0.81 – 1.32	g'	59.670	37	2.0 – 3.0
2	2014 Jan 08	TNT	16:56:17	18:14:52	0.88 – 1.28	:clear	59.670	132	1.0 – 2.0
3	2014 Jan 08	TNT	20:02:05	21:23:39	0.80 – 1.21	:clear	59.670	153	1.2 – 1.5
4	2014 Jan 10	TNT	16:01:33	17:13:00	0.86 – 1.22	r'	55.667	38	1.8 – 3.2
5	2014 Jan 11	TNT	15:47:19	16:36:49	0.92 – 1.17	:z'	43.667	68	1.2 – 1.5
6	2014 Jan 11	TNT	18:58:30	20:16:02	0.87 – 1.25	:$i'+z'$	24.777	122	0.9 – 1.1
7	2014 Jan 11	TNT	21:53:02	23:23:08	0.73 – 1.17	r'	34.777	71	1.4 – 1.8
8	2014 Jan 12	TNT	18:14:40	19:45:29	0.77 – 1.22	:$i'+z'$	12.772	91	1.0 – 1.8
9	2014 Jan 12	TNT	22:03:15	23:10:48	0.90 – 1.24	:KG5	49.777	85	1.2 – 1.4
10	2014 Jan 15	TNT	20:21:41	22:22:30	0.78 – 1.38	:r'	58.777	17	2.0 – 3.0
11	2014 Jan 28	TNT	15:04:48	16:37:17	0.83 – 1.29	KG5	9.852	31	1.4 – 2.0
12	2014 Jan 31	TNT	16:54:42	20:29:19	0.75 – 1.81	i'	3.352	38	1.2 – 3.5
13	2014 Feb 11	TNT	19:35:39	21:00:47	0.98 – 1.34	g'	12.777	19	1.6 – 2.1
14	2014 Feb 28	TNT	18:38:05	20:31:30	0.75 – 1.32	g'	3.352	21	1.2 – 2.0
15	2014 Mar 26	TNT	14:56:13	16:47:43	0.89 – 1.44	g'	9.872	27	1.4 – 1.8
16	2014 Mar 29	TNT	13:10:23	15:11:32	0.74 – 1.34	r'	9.852	26	1.2 – 2.2
17	2014 Mar 30	TNT	12:50:12	15:02:53	0.76 – 1.42	g'	3.352	20	1.2 – 2.0
18	2014 Mar 31	TNT	12:32:27	17:26:53	0.80 – 2.26	r'	3.352	24	1.2 – 2.2
19	2014 Apr 01	TNT	12:23:07	17:09:11	0.88 – 2.29	g'	3.352	18	1.3 – 2.0
20	2014 Apr 02	TNT	14:04:14	18:14:38	0.50 – 1.74	:g'	4.852	15	1.2 – 1.8
21	2014 Apr 03	TNT	16:58:35	19:32:28	0.49 – 1.25	r'	3.352	16	1.0 – 2.2
22	2014 Dec 22	TNT	17:09:37	20:29:12	0.30 – 1.29	g'	4.852	22	1.8 – 3.0
23	2015 Jan 01	TNT	20:44:18	23:06:57	0.92 – 1.32	KG5	10.352	52	1.2 – 1.5
24	2015 Jan 12	TNT	20:32:47	21:33:49	0.93 – 1.24	g'	9.876	17	1.6 – 3.0
25	2015 Jan 17	WHT	01:12:31	02:55:59	0.82 – 1.33	$u'g'r'$	12;4;4	48	1.0 – 2.0
26	2015 Feb 19	TNT	16:44:53	19:28:52	0.55 – 1.36	g'	9.352	25	1.0 – 2.2
27	2015 Feb 19	TNT	19:31:20	22:52:28	0.38 – 1.37	r'	9.352	38	1.0 – 2.0
28	2015 Feb 24	TNT	15:47:19	17:08:34	0.89 – 1.29	KG5	9.862	42	1.5 – 2.2
29	2015 Mar 18	TNT	12:57:49	16:06:24	0.79 – 1.72	r'	9.352	14	1.2 – 2.2
30	2015 Mar 18	TNT	16:09:00	19:16:25	0.74 – 1.66	g'	9.352	30	1.2 – 2.2
31	2015 Mar 19	TNT	12:28:51	14:11:28	0.77 – 1.28	i'	6.000	38	1.0 – 1.6
32	2015 Mar 19	TNT	15:38:22	17:44:46	0.71 – 1.33	g'	9.352	29	1.3 – 1.8
33	2015 Mar 19	TNT	18:47:17	20:51:36	0.64 – 1.26	KG5	7.352	32	1.6 – 3.0
34	2015 Mar 20	TNT	12:16:12	13:36:15	0.83 – 1.23	g'	9.352	8	1.6 – 4.0
35	2015 May 12	TNT	12:45:53	15:03:51	0.90 – 1.24	g'	9.352	6	1.9 – 2.6

an initial model. In this model, we allowed the inclination angle, the white dwarf and red dwarf radii, and the red dwarf temperature to vary, while the mass ratio and the white dwarf temperature are fixed. We have excluded those parts of light curves with dips and other variations during the fitting process. The 'hot' solution with 32595 K for the temperature of the white dwarf gives too strong a reflection effect in our model. On the other hand, the lower temperature of 17505 K from the SDSS WDMS binary catalogue is probably also not reliable (it has a very high gravity of $\log(g) = 9.5$ and it is found at the edge of the model grid), but must be closer to the correct value. Hence, we chose the value of 17505 K for our model. The strong contamination by the red dwarf and the faintness of the system are possibly the cause of the uncertainty in the temperature determination.

We also applied a Markov Chain Monte Carlo (MCMC) algorithm to confirm the result of the light curve fit. Using a fixed mass ratio of $q = 0.5$ with white dwarf temperature of $T_{\rm WD} = 17505$ K, our best fit model gives an inclination angle of $i = 85°$. The radii of the two stars (scaled by the binary separation) are $R_{\rm WD}/a = 0.0116$ and $R_{\rm sec}/a = 0.3572$, with the red dwarf companion almost filling its Roche Lobe. The temperatures of the red dwarf star derived from our model is $T_{\rm sec} = 3160$ K. We then fitted each individual light curve using the binary parameters given above, allowing only the orbital period and the time of mid-eclipse as free parameters.

3.2 Mid-eclipse times and new ephemeris

We first adopted the ephemeris from P13 to compute the orbital phase, where the orbital period is $P_{\rm orb}$=0.140359073(1) days. The adopted ephemeris shows that the mid-eclipse is offset earlier by ∼3 min from the expected time. The derived O−C values from ULTRASPEC data taken in late 2014 and 2015 showed a linear but decreasing trend, indicating that the adopted P13's ephemeris is not suitable for our data. We calculated a new ephemeris for J1021+1744 where we

Table 2. The eclipse times for J1021+1744. For each date, we listed the filter names, cycle number, mid-eclipses, the O−C and the uncertainties in our O−C calculation in seconds. The eclipse times of the original and the new LT data are given in the first and second rows. For ULTRACAM data (2015 Jan 17), we list the weighted average of the mid-eclipse times from each filter.

Date	Filter	Cycle number	Mid-eclipse time BMJD(TDB)	O−C (sec)
2012 Jun 15	V+R	-4068	56093.90558(12)	57.99 ± 10.56
			56093.905144(79)	20.34 ± 7.10
2014 Jan 07	g'	0	56664.884326(23)	0 ± 2.82
2014 Jan 08	clear	6	56665.726518(49)	3.40 ± 4.67
2014 Jan 08	clear	7	56665.866817(46)	-1.74 ± 4.42
2014 Jan 10	r'	20	56667.691512(61)	0.91 ± 5.63
2014 Jan 11	z'	27	56668.67420(13)	15.96 ± 11.26
2014 Jan 11	$i'+z'$	28	56668.814482(79)	9.60 ± 7.13
2014 Jan 11	r'	29	56668.954726(50)	-0.37 ± 4.76
2014 Jan 12	$i'+z'$	35	56669.797077(56)	16.80 ± 5.25
2014 Jan 12	KG5	36	56669.937231(17)	-0.88 ± 2.49
2014 Jan 15	r'	57	56672.884782(93)	0.57 ± 8.26
2014 Jan 28	KG5	148	56685.657432(21)	0.87 ± 2.72
2014 Jan 31	i'	170	56688.745118(33)	25.67 ± 3.47
2014 Feb 11	g'	249	56699.833578(47)	-6.79 ± 4.56
2014 Feb 28	g'	370	56716.817073(14)	0.60 ± 2.31
2014 Mar 26	g'	554	56742.643108(20)	2.70 ± 2.65
2014 Mar 29	r'	575	56745.590612(30)	0.09 ± 3.25
2014 Mar 30	g'	582	56746.573142(14)	1.72 ± 2.33
2014 Mar 31	r'	589	56747.555624(31)	-0.81 ± 3.31
2014 Mar 31	r'	590	56747.696023(27)	2.70 ± 3.09
2014 Apr 01	g'	596	56748.538134(22)	-0.94 ± 2.74
2014 Apr 01	g'	597	56748.678507(16)	0.33 ± 2.41
2014 Apr 02	g'	604	56749.660988(22)	-2.25 ± 2.73
2014 Apr 03	r'	612	56750.783865(43)	-1.71 ± 4.25
2014 Dec 22	g'	2486	57013.816200(15)	0.67 ± 2.40
2015 Jan 01	KG5	2558	57023.922030(12)	0.68 ± 2.25
2015 Jan 12	g'	2636	57034.870024(22)	1.59 ± 2.74
2015 Jan 17	$u'g'r'$	2666	57039.0808021(41)	2.28 ± 2.02
2015 Feb 19	g'	2906	57072.766864(12)	-0.45 ± 2.23
2015 Feb 19	r'	2907	57072.907249(20)	1.77 ± 2.66
2015 Feb 24	KG5	2941	57077.679420(20)	-0.49 ± 2.67
2015 Mar 18	r'	3097	57099.575392(27)	-1.38 ± 2.34
2015 Mar 18	g'	3098	57099.715735(14)	-0.031 ± 3.75
2015 Mar 19	i'	3104	57100.557875(56)	0.25 ± 2.38
2015 Mar 19	g'	3105	57100.698265(15)	-2.45 ± 5.26
2015 Mar 19	KG5	3106	57100.838629(24)	0.73 ± 2.87
2015 Mar 20	g'	3111	57101.540570(50)	13.42 ± 4.73
2015 May 12	g'	3489	57154.596013(21)	-0.95 ± 2.71

used a light curve fitting method (as described above) to find the mid-eclipse timings for every light curve. The new orbital period resulting from our fitting process is shorter by almost 0.03 s and the new ephemeris derived from our data is

$$\mathrm{BMJD(TDB)} = 56664.8843262(231) + 0.140358755(1)E$$

We list the mid-eclipse times in Table 2, including the mid-eclipse of the LT light curve of P13. We have applied a barycentric correction to all of our times following a method developed by Eastman et al. (2010), and we present these numbers in BMJD(TDB). The O−C are derived with respect to the T0 on 2014 January 7 (the date of the first ULTRASPEC data obtained at TNT). In Figure 1 we compare the O−C values calculated using P13's orbital period (left panel) with the values from our newly derived orbital period (right panel). P13's LT data point is plotted as a filled square. Additionally, we fitted the LT light curve using our binary model and recalculated the O−C using our ephemeris (presented as filled triangle). There is a 38 seconds difference between the original and the new LT mideclipse times. In their paper, P13 mentioned a flare which occured during the egress of the white dwarf (see Figure 5 of P13). This flare could have affected the fitting of the eclipse in P13. Since we know the width of the eclipse from our ULTRASPEC data, we can exclude the flare in P13 data for our light curve fitting.

3.3 Dips in J1021+1744

We have detected for the first time clear evidence of multiple dips after the main eclipse in the light curve of J1021+1744, as shown in Figure 2. The light curves presented in the figure are the g' filter data of our target and the comparison star (marked as "Ref") taken on the night of 2014 January

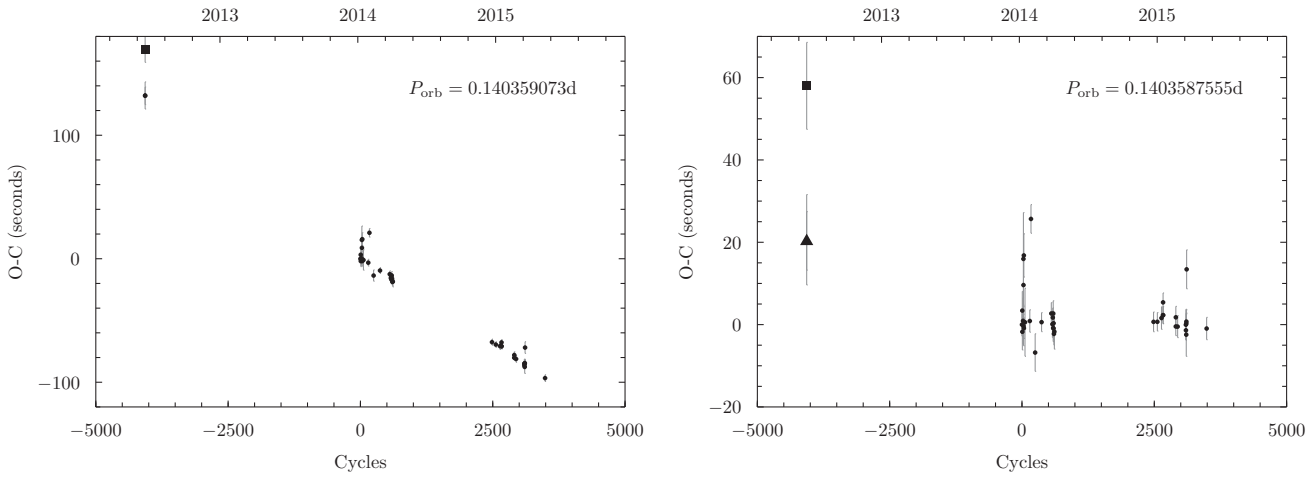

Figure 1. O−C diagrams for J1021+1744 calculated using the old ephemeris of P13 (left) and our new ephemeris from ULTRASPEC data (right). The LT data from P13 is marked with a filled square. Our re-fitting result to the LT data using the ephemeris from ULTRASPEC data is marked with a filled triangle (see section 3.2).

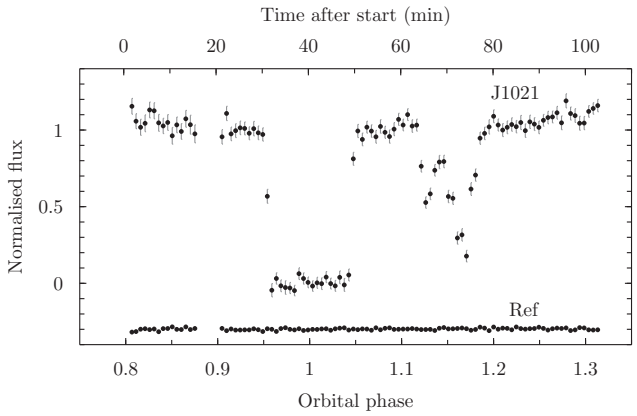

Figure 2. g' filter light curve of J1021+1744 from 2014 January 7, displaying the white dwarf eclipse and double dip from orbital phase 1.1 to 1.2. Each data point represents a single frame with exposure time 59 sec. The small gap around phase 0.89 is due to the rotation of the instrument during the exposure.

7. In this work, we present the light curves in terms of orbital phase, using the ephemeris derived from ULTRASPEC data. For reference, a 0.1 phase interval corresponds to ∼20 minutes.

The flux scale is normalised and then rescaled to 1 outside the eclipse and to 0 during the eclipse. We computed the average values between the orbital phase $0.9-0.95$ and $0.97-1.03$, and used the first phase range for our light curve normalisation. The rescaling factor is the difference between the two average values. We chose to rescale our light curves to minimise the effect of the filters over our analysis of the dips (see below).

We used a similar approach for the light curve of the comparison star shown in Figure 2. We normalised the flux of the comparison star to 1 using the average value in the same phase range mentioned above. The normalized comparison star's flux is then offset to -0.3 for clarity.

The light curve of J1021+1744 clearly shows variations after the white dwarf eclipse, around phase $1.1-1.2$. The drop in our light curve has two connected dips with different depth. The system dims by ∼50% during the first dip, and becomes even fainter through the second dip, with more than 80% of the light of the white dwarf blocked. The star then slowly returns to its out-of-eclipse brightness around phase 1.2. The first dip seems to be consistent in phase and in amplitude with that reported by P13. The second dip however was not present at all in the LT light curve. It should have been clearly evident as it is wider and deeper in our data than the first dip. We suspect that the second dip developed after the P13 observation in 2012 June. We will show later that these dips are evolving in shape and amplitude.

After the initial work to identify the correct filter, the wavelength-dependence of the primary eclipses of J1021+1744 follow our expectations for this type of binaries. The eclipses are dominant in the blue and decrease in depth towards the red part of the spectrum. The trend in wavelength for the dip features is the same as in the main eclipse, and possibly even more pronounced. The dips are obscuration of the white dwarf, hence the similarity in the wavelength dependency between the eclipses and the dips. Later data taken (simultaneously) using ULTRACAM show that the dips are deepest in the u' band, as illustrated in Figure 3. The ULTRACAM u' band data were taken with a longer exposure time compared to the g' or r' filters, therefore we have smaller number of datapoints in the u' band light curve. For these data, the sampling in the u' filter is three times slower than in the other filters. We normalised the flux scale to the average value of the pre-eclipse section only (phase $0.90-0.95$) to show the relative shape and the depth of the white dwarf eclipses. We would like to note that the ULTRACAM data definitely confirms the dip depths as a function of wavelength, as the ULTRASPEC data were taken in different orbits for different filters.

The dips are clearly seen in the g' filter, though they appear to be less prominent at this wavelength. They are shallower in r' and KG5 filters, and barely visible in the i' and $i'+z'$ filters. This may suggest that the material causing these dips has an optical thickness decreasing towards the red part of the spectrum.

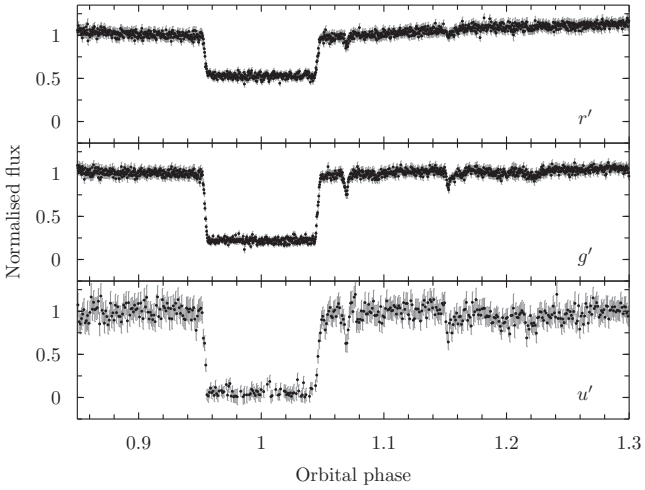

Figure 3. Light curve of J1021+1744 taken on 2015 January 17 from the WHT telescope with ULTRACAM. From top to bottom the filters are r', g', and u'. The data in u' has fewer points due to longer exposure time. The light curves are normalised to the average flux between phase 0.9−0.95. The white dwarf eclipses follow the expected pattern where they are deeper at bluer wavelengths. The dip features seem to follow a similar trend.

Our next task was to examine the dips profile. Since the mid-eclipse times are known, the location of the dips can be determined accurately. In our 2014 data, the dips were prominent and were always located between phase 1.10 and 1.25. Multiple number of dips are recorded in every light curve, often with complex shapes. We present the light curves obtained between 2014 January−April in Figure 4, focusing on the section where the dips are visible. The light curves are ordered in time from top to bottom. We exclude the data in the i', z', $i'+z'$ filters because the dips are faint in these wavelengths, as well as the data taken in the night of 2014 April 3. Our target was setting with airmass >2 during our observation on 2014 April 3, and the part of light curve with dips is heavily affected by noise. Figure 4 shows 18 light curves and the flux of each light curve has been rescaled to 0 and 1, as in Figure 2. For the nights where we used a short exposure time (<5 s), the data points are binned to show more clearly the profile of the dips.

The analysis of the dips in J1021+1744 is quite challenging, due to the fact that they were evolving rapidly in time (as seen in Figure 4) and in shape, from one simple structure into a complex one or vice versa. We decided to mark the well-visible dips, but only those which can be seen in almost every light curve. We used a numbering system from 1 to 5 based on their position in orbital phase. The number can be followed by letters a, b, and c for a dip which is split into a few smaller dips (in the case of dip 1).

Dips 1 and 3 are always present in our 2014 data. We marked dip 1 as '$1_{\rm b}$' for the first seven light curves, and then assign the letters 'a' and 'b' after it split into two narrow dips. Dip 2 was marked for the first time on 2014 Jan 15, although, it is possible that this dip was already present in the light curves prior to this date. However, the long exposure used for the first few light curves does not allow us to resolve this dip. Dips 4 and 5 were not present at all at the beginning of our observations. They first emerged on 2014 January 28 and then disappear and reappear throughout 2014. There were two occasions where another dip appeared between dips 1 and 2, which was on March 30 and April 1. This dip is marked as '$1_{\rm c}$'. Dip $1_{\rm c}$ is a fine example to show the swift evolution of the dips. On the night of 2014 April 1, we observed J1021+1744 uninterruptedly for 5 hours, following two eclipses in orbital cycle 596 and 597. During this observation, we witnessed the appearance of dip 1c in cycle 597, blocking half of the total light from the binary for more than two minutes. Such a dip was not recorded in the light curve of cycle 596.

We followed the same procedure to mark the dips in our 2015 data (Figure 5). It is obvious that the dips which were present in our 2015 light curves are different from those that appeared in our 2014 data. We obtained our first data of the second observing season on the night of 2014 December 22. The dip was absent from this light curve. A small dip seems to be visible at phase 1.07 on 2015 January 1 and January 12. However, we are not certain of this because it lies far (in phase) from the previous known dips in this system. It is also only marginally significant given the errors and the fluctuations in the light curves. Our WHT+ULTRACAM data, which was taken four nights later, confirmed the presence of this small dip. This light curve also revealed a second shallow dip at phase ∼1.15 and possibly even a third dip at phase ∼1.22. Our further TNT observations show that only dip 2 which remains present in our subsequent 2015 data.

4 DISCUSSION

Our data set is sufficiently extended, and the number and positions of the dips sufficiently complex, that it is difficult to provide a detailed discussion of each feature. However, we can discuss in broad terms at least the time scale of the phenomenon and the time evolution of the dips, in order to infer some conclusions.

We counted the total number of dips in each light curve based on the markings given in Figure 4 and 5, where each mark represent one dip. In some light curves we assigned '$_{\rm a}1_{\rm b}$' and this mark is counted as two dips. The result is shown in Figure 6 (top panels). In 2014, we found that there are dips in every light curve, starting with two and increasing to about five or more by 2014 April. The actual number varies from day to day, even from one cycle to another. The light curves with the highest number of dips are the g'-band light curves on 2014 March 30 and April 1, where we counted 7 dips in each dataset. For our 2015 observations, on the other hand, only the ULTRACAM data showed two, possibly three, dips. We marked only dip 1 and 2 in the ULTRACAM data because the third dip was very weak and was not seen in the other light curves (possibly due to less resolution in the TNT data). Five other datasets show only one small dip, and the rest (marked with grey crosses) have no dip feature. Given the large gap between the two data sets (over 8 months without any data), it is not possible to say whether the dips seen in 2014 evolved into those seen in 2015. At the very least, we can state that the dips had a lifetime of about three months: they were well developed when we first detected them in 2014 January, and showed no signs of abating by April. If, on the other hand, we assume that the dips were indeed present and evolving between

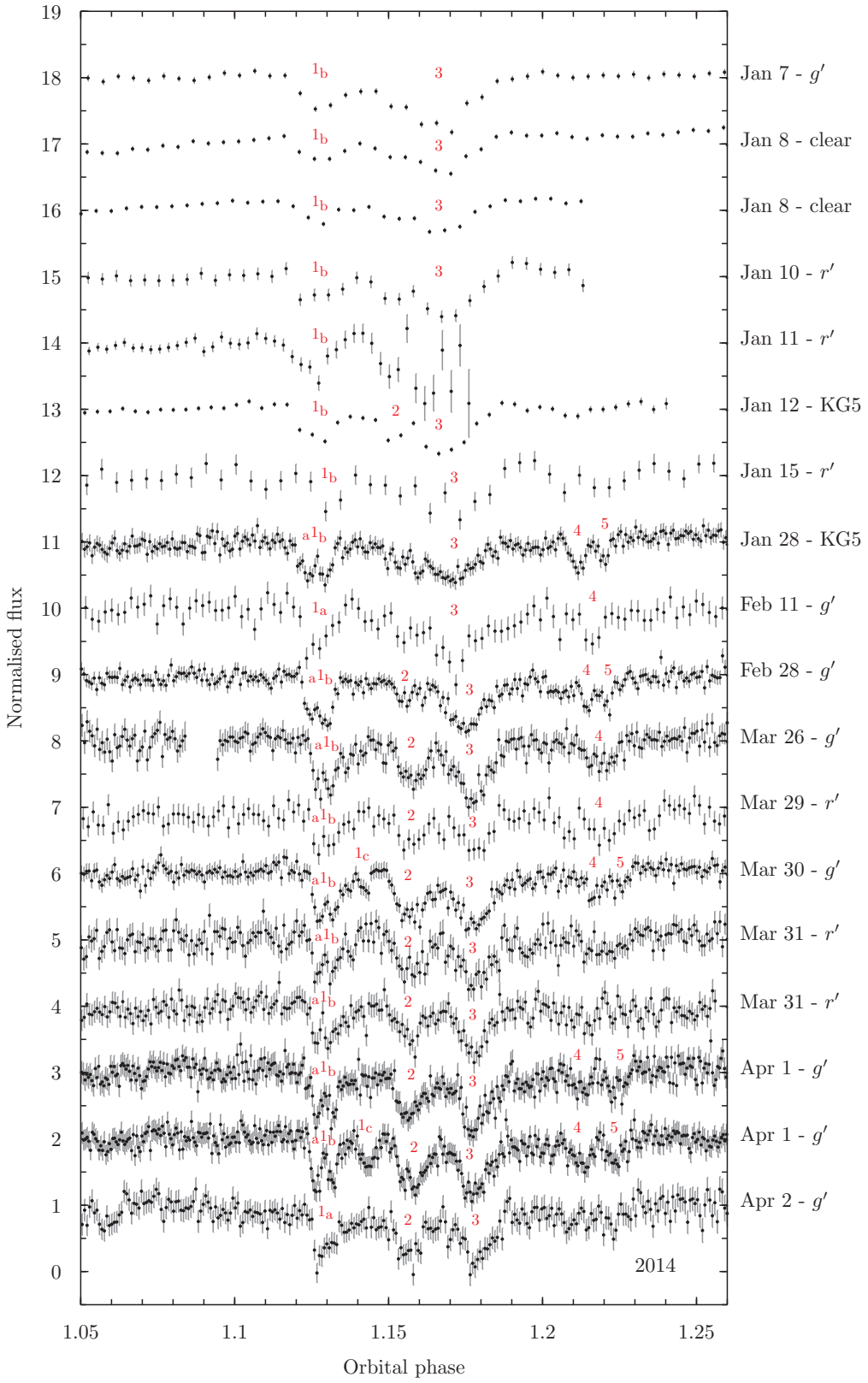

Figure 4. A close up look of the light curves of J1021+1744 (2014 data) between phases $1.05-1.26$. The light curves are arranged from the oldest at the top to the newest at the bottom. Some data with short exposure times are binned for clarity. The dips in our 2014 light curves clearly evolves in shape, width, and depth. We mark the position of each dip with numbers from 1 to 5. In some light curves where dip 1 is split into three smaller dips, we annotated them with 1_a, 1_b and 1_c. Each mark represents one dip, except for ${}_a1_b$ where we count two dips. The total number of dips for each light curve is counted based on these marks.

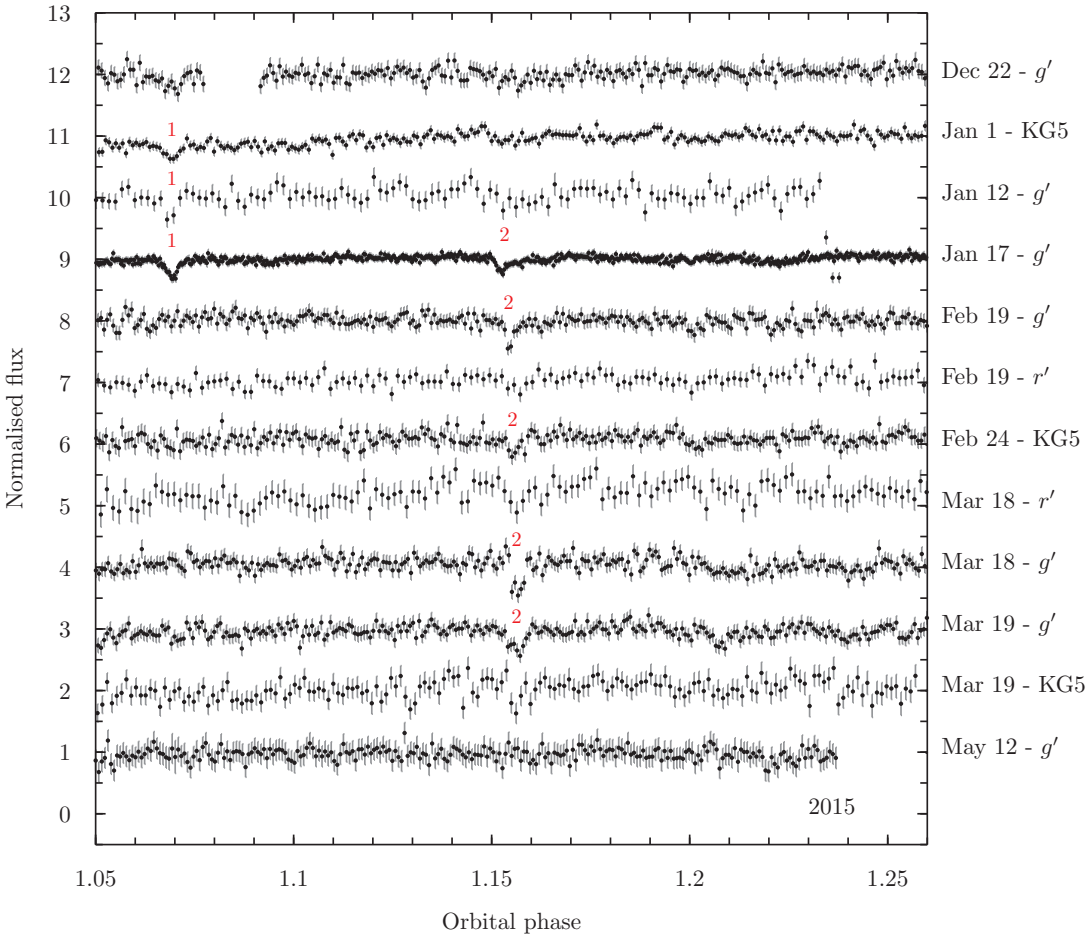

Figure 5. Similar to Figure 4, but for the data obtained in 2015 observing season. The first data were taken on 2014 December 22. Only one or two small dips are seen in some light curves. The light curves with the highest time-resolution have been binned for clarity.

April and December, then their minimum lifetime would be at least 1.5 years. A connection with the first detected dip by P13, implying a lifetime of several years, seems more difficult to defend. We recall the case of QS Vir (O'Donoghue et al. 2003), in which two deep dips were detected before the primary eclipse. However, further observations did not detect the dips again, pointing to a short-lived phenomenon.

In Figure 6 we also plot the position of the dips in the 2014 and 2015 data (bottom panels). To measure the positions, we visually inspected each dip and tried to determine the minimum of each feature, unless they had an asymmetric shape. In this case we used the position of the data points with the lowest flux. Our analysis shows that all dips were shifting towards later orbital phase, although, small variations exist in the early 2014 data. From this plot we can infer that the dips are not stationary with respect to the orbital phase of the binary. It might also imply that the material is slowly drifting away from the binary. We measure a shift of 0.01 in orbital phase for dip 3, or almost 2 minutes in time. Despite having different characteristics (in depth, width, and numbers), the dips from our 2015 datasets also show similar behaviour. The fact that the dips are multiple and are shifting in phase leads to the conclusion that the material is in the form of several blobs, which are orbiting the red dwarf but at the same time subject to varying gravitational forces which change their relative position from the star and among themselves.

Our evaluation of the depth and the width of the dips are presented in Figure 7. The measurement was done for the 2014 data (except dips 1c). We calculated the flux at the position/phase measured in Figure 6. The width is measured at the level where the normalised flux is equal to 1. In the case of connecting dips, such as dips 1_a–1_b and dips 2–3, the flux values between the dips are often lower than 1. For this situation, we mark the start (or the end) of one dip at the phase with the highest flux between the two dips.

The intensity plots show a similar feature where all of the dips are found to fluctuate on short time scale (days). This fluctuation can be seen clearly for dips 1b and 3 after cycle 550 in all of the dips. This short time scale variability is also seen in the plots of the width of the dips. These variations are also seen in the intensity and width plots during cycle 0–57. However, the small fluctuations are much harder to detect with the longer integration time, and the width is also difficult to be measured accurately. Hence, we faded out the data points for the first few light curves in 2014 January (cycle 0–57) as these points have larger uncertainties compared to the rest of the data. For both the intensity and the width plots, we only have three data points (taken in Jan 28, Feb 11, and Feb 28) between cycle 50 and cycle 550. There-

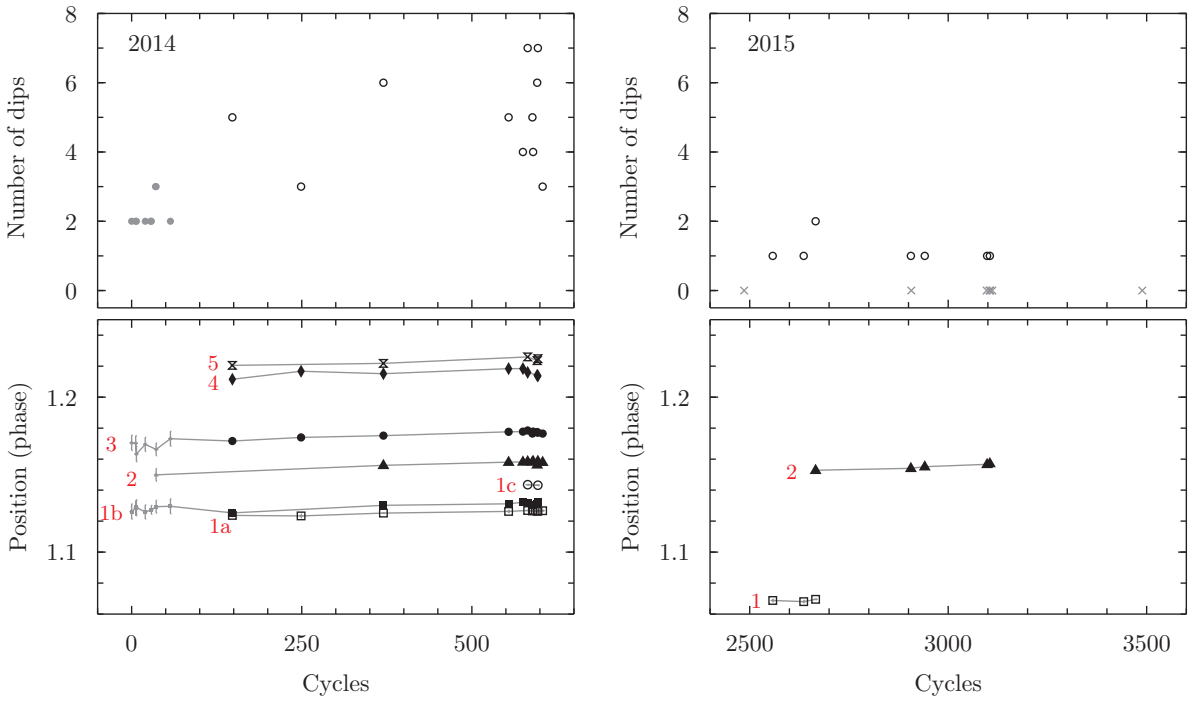

Figure 6. Top panels: The total number of dips seen in each light curve in 2014 (left) and 2015 (right). The grey dots on the left panel represent the number of dips in the light curves taken with integration times longer than 30 seconds. The grey crosses on the right panel mark the orbital cycles where the dips are absent in the light curve. Bottom panels: The position of each dip in orbital phase. The data with longer exposures taken between Jan 7 − 15 are faded out with grey error bars.

fore, we cannot tell whether there was any short time-scale variability during that period.

We note that potentially similar dips were observed before in QS Vir (O'Donoghue et al. 2003) in the optical, and in V471 Tau (Jensen et al. 1986) in X-rays. However, this is the first time that such dips are well resolved in time and monitored over about 1.5 years at several wavelengths. The dips in QS Vir were also detected spectroscopically by Parsons et al. (2011), altough the material was not optically thick. Therefore, the dips in QS Vir as reported by the authors were seen only in the lines and not in the continuum light. In Figure 8 we show the expected location of the dips in J1021+1744 as observed on 2014 April 1, where they seem to cluster near the L5 point. Only little force is needed to hold material at an equilibrium point, which might explain why we found the materials in J1021+1744 near the Lagrange L5 point. Opposite to the usual convention, the binary rotates clockwise in this figure.

It is interesting that in QS Vir and V471 Tau the dips are also reported to be in a very similar location close to the L4/L5 "trojan" points. Jensen et al. (1986) found that the X-ray dips in V471 Tau were seen near both L4 and L5 points, while the prominence material in QS Vir is located close to its L5 point (Parsons et al. 2011).

As a last remark, we report that we could, in a few cases, monitor J1021+1744 over a full orbit (see entries no 12, 18, and 19 in Table 1). The data were taken in i', r', and g', consecutively. Two such light curves are presented in Figure 9. We, unfortunately, were unable to detect the dips' material passing in front of the M dwarf. The secondary eclipse was also undetectable in any filter. We note however that on March 31 we observed a significant brightening, visible around phase 0.72. The total intensity appeared to double and fade back within a few minutes. This is interpreted as a flare from the red dwarf, pointing to significant chromospheric activity. Whether such active behaviour is partly responsible for mass ejections, which could funnel material to the observed dip positions, is an interesting possibility.

5 CONCLUSION

We have detected the signature of dips in the light curve of the detached, eclipsing white dwarf/M dwarf binary SDSS J1021+1744. Although potentially similar dips were seen before in a few other stars, such as in QS Vir (O'Donoghue et al. 2003) and in V471 Tau (Jensen et al. 1986), this is the first time that such dips are well resolved in time and monitored over about 1.5 years in various filters across the whole visible spectrum. The dips are at locations which appear consistent with being close to the L5 point.

Our observations show that the dips are visible over hundreds of orbits, from a minimum of 3 months, possibly up to 4−6 months and even up to 3 years. They also clearly reveal a complex dip structure, with their number, depth, and shape changing in time and as a function of wavelength. The dip lifetimes are 3−100 times longer lived than prominences on the Sun. On the other hand, the obscuration is probably also comparably larger, suggesting significant mass and density of the blobs. It is noteworthy that the dips have depths of as much as 30% of the total light in the u' and g' band, showing that the material absorbs continuum and not just emission lines as in the case of the Sun.

The origin of these dips, which we speculate is in the

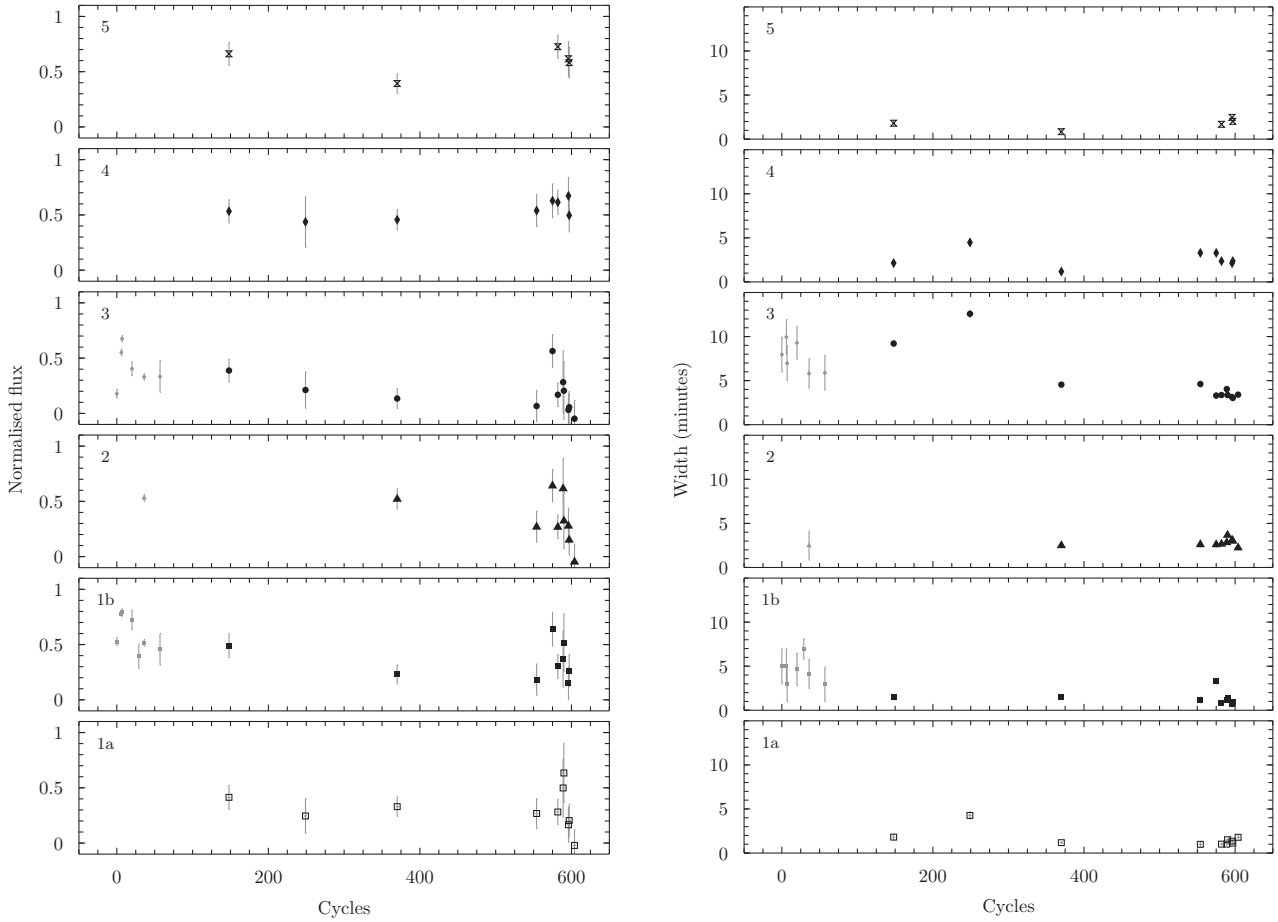

Figure 7. The plot of the flux (left) and the width (right) of the dips during the 2014 observation. The flux is rescaled to 0 during eclipse and 1 outside the eclipse (see text for details). In this manner, a value of 0 shows that there is more light being blocked by the dip. The out-of-eclipse part in the r' filter is slightly higher due to the contribution from the secondary star, and the dips are shallower in the red filter. The width is measured at the top of the dips. The grey points (see 1b, 2 and 3) are for data with larger uncertainties (due to longer integration times and less resolution) obtained between January $7-15$.

form of blobs of gas or very extended prominences from the red dwarf star, is a new phenomenon to be reckoned with in models of PCEBs. Future monitoring of this binary, and other similar systems, is of crucial importance to understand the frequency of these occurrences and to learn more about their nature.

We have also provided a new ephemeris for the binary system, significantly improved over that of P13 thanks to a much longer time span. At the accuracy level of our data, where the majority of the data in the O−C diagram are scattered within ±10 seconds from the zero value, we find no evidence of changes in the primary mid-eclipse times.

ACKNOWLEDGMENTS

We thank the anonymous referee for valuable comments and suggestions which helped improved this paper. We also thank Boris Gaensicke for useful discussions. PI acknowledges the support from NRC-Thailand and a Royal Society International Exchange. TRM acknowledges the support of the Royal Society International Exchange Grant and of the Science and Technology Facilities Council under grant number ST/L000733. NS and KC would like to thank Suranaree University of Technology and the Office of Higher Education Commission for the partial support under the NRU project. SGP acknowledges financial support from FONDECYT in the form of grant number 3140585. This work has made use of data obtained at the Thai National Observatory on Doi Inthanon, operated by NARIT, and the WHT on La Palma.

REFERENCES

Abazajian K. N., et al., 2009, ApJS, 182, 543
Briggs G. P., Ferrario L., Tout C. A., Wickramasinghe D. T., Hurley J. R., 2015, MNRAS, 447, 1713
Copperwheat C. M., Marsh T. R., Dhillon V. S., Littlefair S. P., Hickman R., Gänsicke B. T., Southworth J., 2010, MNRAS, 402, 1824
Dhillon V. S., et al., 2007, MNRAS, 378, 825
Dhillon V. S., et al., 2014, MNRAS, 444, 4009
Drake A. J., et al., 2009, ApJ, 696, 870
Drake A. J., et al., 2014, MNRAS, 441, 1186
Eastman J., Siverd R., Gaudi B. S., 2010, PASP, 122, 935
Jensen K. A., Swank J. H., Petre R., Guinan E. F., Sion E. M., Shipman H. L., 1986, ApJ, 309, L27
Marsh T. R., 2000, New Astron. Rev., 44, 119

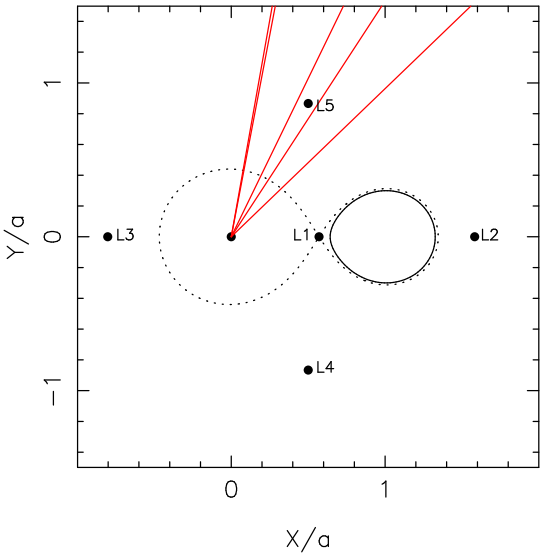

Figure 8. The Roche geometry of J1021+1744, scaled by the separation of the two stars. The dotted lines indicate the Roche lobe, while L1–L5 mark the positions of the Lagrangian points in this binary. The red dwarf star (solid black line) is seen very close to filling its Roche lobe. The straight lines indicate the line of sight to the white dwarf where the dips are seen on 2014 April 1. The binary rotates in clockwise direction.

O'Donoghue D., Koen C., Kilkenny D., Stobie R. S., Koester D., Bessell M. S., Hambly N., MacGillivray H., 2003, MNRAS, 345, 506
Parsons S. G., Marsh T. R., Gänsicke B. T., Tappert C., 2011, MNRAS, 412, 2563
Parsons S. G., et al., 2013, MNRAS, 429, 256
Parsons S. G., et al., 2015, MNRAS, 449, 2194
Rebassa-Mansergas A., Gänsicke B. T., Rodríguez-Gil P., Schreiber M. R., Koester D., 2007, MNRAS, 382, 1377
Rebassa-Mansergas A., Nebot Gómez-Morán A., Schreiber M. R., Gänsicke B. T., Schwope A., Gallardo J., Koester D., 2012, MNRAS, 419, 806
Rebassa-Mansergas A., Agurto-Gangas C., Schreiber M. R., Gänsicke B. T., Koester D., 2013, MNRAS, 433, 3398
Webbink R. F., 1984, ApJ, 277, 355
York D. G., et al., 2000, AJ, 120, 1579

This paper has been typeset from a TEX/LATEX file prepared by the author.

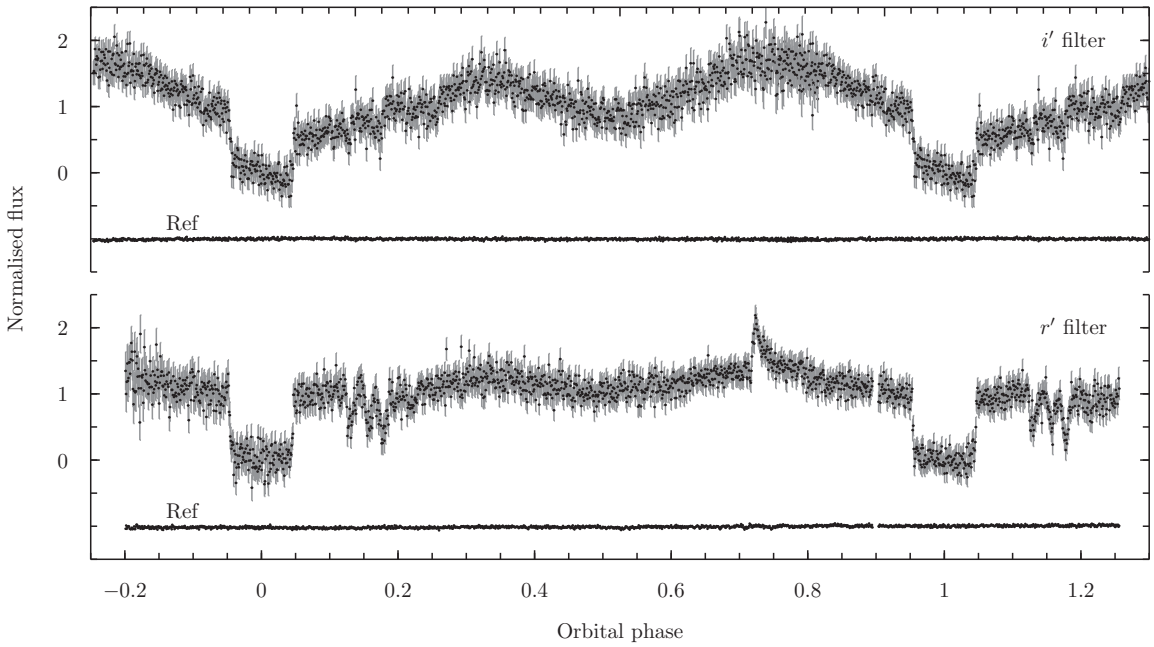

Figure 9. Full orbit light curves in r' (2014 Mar 31) and i' (2014 Jan 31) filters. The y-axis are scaled to 0 during the eclipse and 1 on the out-of-eclipse part (see text). The light curves of the reference star are marked as "Ref". Ellipsoidal modulation is seen in both light curves, however this effect is more dominant in the i' filter. The r'-band light curve also exhibit a large flaring event at phase ∼0.72. There is no apparent signature from the low-mass star around orbital phase 0.5.